Distance and Wavelength Dependent Quenching of Molecular Fluorescence by Au@SiO_2 Core–Shell Nanoparticles

Philipp Reineck,[†] Daniel Gómez,[‡,§,⊥] Soon Hock Ng,[†] Matthias Karg,[¶] Toby Bell,[#] Paul Mulvaney,[▽,*] and Udo Bach[†,‡,§,*]

[†]Department of Materials Engineering, Faculty of Engineering and [#]School of Chemistry, Faculty of Science, Monash University, Clayton, 3800, VIC, Australia, [‡]Materials Science and Engineering, Commonwealth Scientific and Industrial Research Organization, Clayton South, Victoria 3169, Australia, [§]The Melbourne Centre for Nanofabrication, 151 Wellington Road, Clayton 3168, Victoria, Australia, [⊥]School of Physics and [▽]School of Chemistry & Bio21 Institute, University of Melbourne, Parkville, 3010, Victoria, Australia, and [¶]Physical Chemistry Department, University of Bayreuth, Universitätsstrasse 30, 95440 Bayreuth, Germany

ABSTRACT Gold nanoparticles and nearby fluorophores interact *via* electromagnetic coupling upon light excitation. We determine the distance and wavelength dependence of this coupling theoretically and experimentally *via* steady-state and time-resolved fluorescence spectroscopy. For the first time, the fluorescence quenching of four different dye molecules, which absorb light at different wavelengths across the visible spectrum and into the near-infrared, is studied using a rigid silica shell as a spacer. A comprehensive experimental determination of the distance dependence from complete quenching to no coupling is carried out by a systematic variation of the silica shell thickness. Electrodynamic theory predicts the observed quenching quantitatively in terms of energy transfer from the molecular emitter to the gold nanoparticle. The plasmonic field enhancement in the vicinity of the 13 nm gold nanoparticles is calculated as a function of distance and excitation wavelength and is included in all calculations. Relative radiative and energy transfer rates are determined experimentally and are in good agreement with calculated rates. We demonstrate and quantify the severe effect of dye–dye interactions on the fluorescence properties of dyes attached to the surface of a silica nanoparticle in control experiments. This allows us to determine the experimental conditions, under which dye–dye interactions do not affect the experimental results.

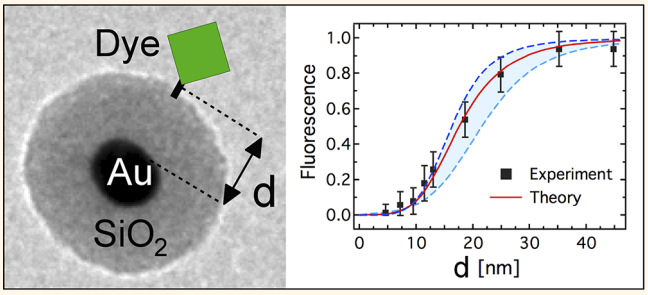

KEYWORDS: gold nanoparticles · plasmonics · dye-nanoparticle interaction · electromagnetic coupling · energy transfer

Visible light excites localized surface plasmon resonances (LSPR) in metal nanoparticles. At this resonance wavelength, gold nanoparticles (Au NPs) both scatter and absorb incident light very efficiently. At the same time, the excitation of a LSPR results in an enhanced electromagnetic near-field in the vicinity of the nanoparticle.[1,2] This enhanced near-field is important because it "focuses" light on a length scale far below the wavelength of light and provides a means to use gold nanoparticles as nanoscale energy transfer antennae in various applications.[3−7] The interactions of the near-field of an Au NP with nearby excited states of fluorescent dye molecules, provides an important model for exploring the possibilities and limitations of nanoscale energy transfer.

However, experimental quantification of the electromagnetic coupling between a gold nanoparticle and a dye molecule is difficult. There are two fundamental challenges. First, it is necessary to distinguish near-field coupling between dye molecules and gold nanoparticles from far field effects. In general, nanoparticles larger than about 50 nm scatter visible light significantly. Therefore, their strong absorption and scattering must be distinguished experimentally from fluorescence quenching and enhancements, respectively. Second, it is important to separate energy transfer from all other possible nonradiative decay pathways (Scheme 1). It is impossible to fix the position of a molecule close to a nanoparticle without changing its local environment with respect to the free molecule in solution. In the

* Address correspondence to udo.bach@monash.edu; mulvaney@unimelb.edu.au.

Received for review January 9, 2013 and accepted May 28, 2013.

Published online May 28, 2013
10.1021/nn401775e

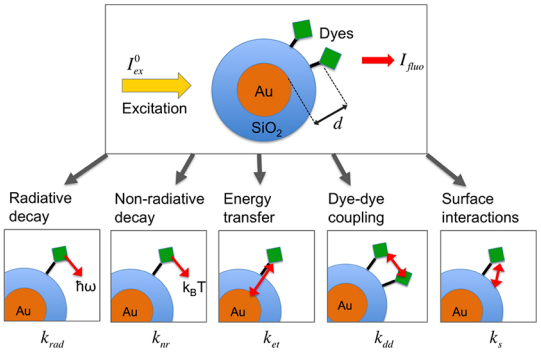

Scheme 1. Possible relaxation pathways for excited fluorescent dye molecules, bound to the silica shell of an Au@SiO_2 core−shell nanoparticle. The separation between gold nanoparticle surface and dye (*d*) is assumed to be the silica shell thickness plus 1 nm to account for the length of the linker molecule ((3-aminopropyl)triethoxysilane) and the dye's functional group.

absence of any electromagnetic coupling, this change in local environment alone can significantly alter the molecule's excited state decay pathways and must be accounted for experimentally. These changes in lifetime or radiative quantum yield can be caused by interactions of the probe dye with the nanoparticle surface or with other neighboring adsorbed dye molecules on the particle surface.

There have been numerous studies of gold nanoparticle-induced quenching and enhancements, including both single molecule experiments[8−13] and ensemble measurements in bulk solution.[14−21] Generally, fluorescence quenching is observed in both types of experiments for nanoparticles smaller than 20 nm.[12−19] However, both fluorescence enhancement and quenching have been observed as a function of distance for strongly scattering 80 nm and larger gold nanoparticles in single particle experiments.[9−11] Whether purely scattering particles of the same size, such as silica nanoparticles, which do not exhibit a LSPR, can also cause fluorescence enhancements has not been investigated to date. In the majority of single molecule and ensemble measurements, organic molecules such as polymers or DNA, are used as spacers to separate the gold particles and dye molecules. Feldmann *et al*. have observed strong fluorescence quenching and shorter fluorescence lifetimes for a dye emitting at 670 nm in the presence of 12 nm gold nanoparticles.[15] Here as well as in many other reports, DNA was used as a linker and spacer molecule between nanoparticle and dye and strong quenching was observed even for the largest separation investigated (16 nm).[15] Significantly weaker quenching has been reported recently by Tinnefeld *et al*. who employed a dye emitting in the same spectral region in single molecule experiments.[13] Gold particles of similar size have also been found to reduce the fluorescence lifetime and intensity of fluorophores, if these emit photons close to the LSPR wavelength of the gold nanoparticles (530 nm).[12] These effects were also observed in single molecule experiments—again using DNA as a spacer molecule. Using molecular spacers, precise distance control can be challenging, and the separations that can be achieved are often limited by the persistence length of the linker molecule. The conductivity of DNA is still a matter of debate[22] and may have an impact on experimental results, especially at short Au NP−dye distances. Also, if more than one dye molecule is attached to a nanoparticle, dye−dye interactions can cause pronounced fluorescence quenching and lifetime shortening as we demonstrate in this study. This effect is notoriously difficult to quantify in the Au NP−dye system and has therefore not been taken into account in previous studies.

Theoretical predictions for the fluorescence intensity quenching or enhancement of a molecular emitter by a gold nanoparticle are generally in qualitative agreement with experimental results.[9−15] The model proposed by Gersten and Nitzan[23] has been employed successfully to rationalize experimental findings.[13−15] In very few publications to date are radiative decay and energy transfer rates determined experimentally and compared to theoretical results. However, identifying the effect of the electromagnetic coupling between dye and Au NP on the decay rate is indispensable for our understanding of the underlying mechanisms. For small nonplasmonic gold nanoparticles of 1.5 nm, a theory referred to as "nanosurface energy transfer" (NSET) has been shown to predict the quenching of fluorophores.[19,24] Here, the quenching obeys a simple $1/d^4$ distance dependence in analogy to the $1/d^6$ distance dependence that governs Förster resonance energy transfer between fluorophores. However, NSET theory has been reported to underestimate the quenching of plasmonic nanoparticles of about 10 nm diameter.[13,16]

Gold nanoparticles between 10 and 20 nm in diameter are important because they are too small to scatter light significantly, but exhibit a well-defined LSPR and an enhanced electromagnetic near-field. It is established that fluorescence of molecules in close proximity to these particles is quenched. Yet, the experimental observation of the complete transition from strong quenching to a full recovery of fluorescence as a function of dye−nanoparticle separation has not been reported for particles in this size regime. The recovery for large separations is crucial as it indicates that no other deactivation mechanisms, except the ones intrinsic to the molecule, are present.

In this report we experimentally observe and analyze this complete transition for 4 different fluorophores. We show that both the fluorescence quenching and lifetime shortening of molecular fluorescence by a 13 nm gold particle are quantitatively predicted by electrodynamic theory. The enhanced electric near-field in the vicinity of the Au NP as well as modifications

to the fluorophore's decay rates due to electromagnetic coupling with the Au NP are included in all calculations. Radiative decay and energy transfer rates are determined from experiments and found to be in agreement with the rates predicted by our model. Spherical gold nanoparticles are coated with insulating silica shells (Au@SiO_2 NPs), which act as a rigid, chemically inert, and electronically insulating spacer between gold core and fluorophore. The shell thickness is tuned precisely *via* a wet chemical growth process and verified through the analysis of transmission electron microscopy (TEM) images. For the first time, Au NP−dye distances are continuously varied from 4 to 43 nm for four different dye molecules throughout the visible to the near-infrared region in ensemble measurements in solution. Within this distance range we are able to observe the transition from almost complete (>90%) quenching at short separations to negligible electromagnetic coupling at a distance of 43 nm. In contrast to most previous studies, we focus on fluorophores, which absorb and emit light close to the Au NP LSPR wavelength, where the strongest electromagnetic coupling is expected. Silica nanoparticles without a metal core are used to study both the effect of dye−dye interactions and the effect of the dye's attachment to the nanoparticle surface on its luminescence in control experiments.

RESULTS AND DISCUSSION

In the simplest model of molecular fluorescence, an excited dye molecule can return to its ground state by emitting a photon or *via* a nonradiative decay pathway such as internal conversion. The fluorescence quantum yield (Q) and fluorescence lifetime (τ) are in this case given by the rate constants that characterize the radiative (k_{rad}) and nonradiative decay (k_{nr}):

$$Q = \frac{k_{rad}}{k_{rad} + k_{nr}} = k_{rad}\tau \qquad (1)$$

For a free dye molecule in solution, nonradiative decay is usually caused by an internal conversion of the excited state energy of the dye to molecular vibrations, by intersystem crossing to the triplet state or by collisional quenching with molecular quenchers such as oxygen. However, when the fluorophore is attached to a metallic nanoparticle and is located in close vicinity to other dye molecules, more excited state deactivation processes become relevant (Scheme 1) and eq 1 must be modified to take these pathways into account:

$$Q = \frac{k_{rad}}{k_{rad} + k_{nr} + k_{et} + k_{dd} + k_s} \qquad (2)$$

Here k_{et} is the rate of energy transfer between NP and dye, k_{dd} the energy transfer rate between dyes on the NP surface, and k_s the rate for excited state relaxation through dye−surface interactions (see Scheme 1). The fluorescence intensity (I_{fluo}) detected by an experimental setup with the photon collection efficiency η also depends on the excitation intensity (I_{ex}) and can be expressed as $I_{fluo} = I_{ex}\eta Q$. In this study, the fluorescence intensity and lifetime of a dye bound to a Au@SiO_2 NP is analyzed with respect to two reference samples and the corresponding fluorescence intensity I_{fluo}^0, which accounts for the optical attenuation of the excitation by the Au NPs and the effect of the dye-surface interactions (see section "Experiments" for details). Since the collection efficiency can be assumed to be the same in all experiments, the detected relative fluorescence intensity reads

$$\frac{I_{fluo}}{I_{fluo}^0} = \frac{I_{ex}}{I_{ex}^0}\frac{Q}{Q^0} \qquad (3)$$

where I_{ex}/I_{ex}^0 is the excitation intensity at the position of the dye molecule relative to the intensity of the incident electromagnetic field. In this way, the enhanced excitation of the dye molecule by the gold NP's enhanced electric near-field is accounted for.

The main goal of the present work is to determine the relative changes in k_{rad} and k_{et} as a function of Au NP-dye separation and peak emission wavelength of the molecular emitter. To be able to do so, I_{ex}/I_{ex}^0, k_{nr}, k_{dd} and k_s must either be known or assumed to be negligibly small. In the following, all four quantities will be analyzed for the Au NP−dye system under investigation. We will show that k_{dd} can have a particularly strong impact on measurements, and we will also determine the conditions under which it becomes negligible.

Au@SiO_2 Nanoparticles and Fluorescent Dyes. Transmission electron micrographs of nanoparticles with different shell thicknesses are shown in Figures 1A−C. Even in the case of the thinnest SiO_2 shell, the shell is clearly visible surrounding the metal core and despite small variations in thickness, no particles with incomplete shells were found. In general, variations in shell thickness were found to be small (0.8 nm average standard deviation) yielding highly monodisperse Au@SiO_2 core−shell nanoparticles (Figure 1D). The fluorescent dye molecules were chosen to investigate three different coupling regimes (Figure 1E): (1) The fluorescence emission peak coincides with the localized surface plasmon resonance (LSPR) absorption peak of the Au@SiO_2 NPs (Atto 488). (2) Absorption spectrum of dye and metal NP strongly overlap and the dye fluorescence is red-shifted from the metal NPs LSPR band (Atto 532, Atto 565). (3) Insignificant overlap of dye and Au NP absorption (Alexa 700). In cases 1 and 2, pronounced electromagnetic coupling between dye and Au NP is expected, while significantly weaker interactions are expected in case 3 due to the difference between the energy of the localized surface plasmon resonance and that of the oscillating molecular emitter.

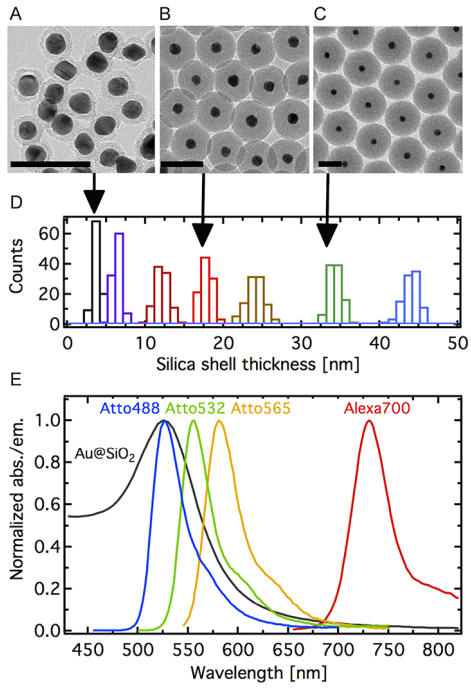

Figure 1. (A–C) Transmission electron microscopy images of Au@SiO_2 core–shell nanoparticles with 12.7 ± 0.3 nm Au cores and 3.6 ± 0.5 nm (A), 17.6 ± 0.7 nm (B), and 34 ± 1.0 nm thick (C) silica shells. Scale bar in all images: 50 nm. (D) Histogram showing the silica shell thickness distribution of the different particles used. The distribution for particles with shell thicknesses of 8.5 and 10.4 nm are not shown for clarity. (E) Emission spectra of the dyes investigated and a typical extinction spectrum of Au@SiO_2 nanoparticles (shell thickness: 8.5 nm). Solvent: ethanol. See Supporting Information for published dye structures and exact SiO_2 shell thicknesses with standard deviations.

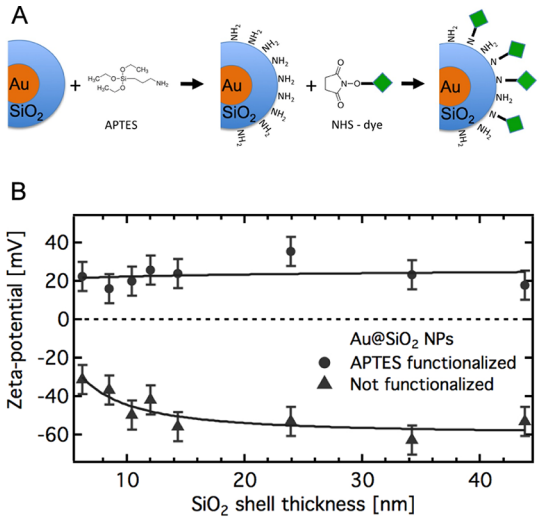

Figure 2. (A) Functionalization of the Au@SiO_2 nanoparticles with (3-aminopropyl)triethoxysilane (APTES) in ethanol, followed by the binding of a *N*-hydroxysuccinimide (NHS)-modified dye molecule to the amine moieties on the NP surface. (B) Zeta potential of Au@SiO_2 before and after the APTES functionalization.

Nanoparticle Functionalization and Dye Attachment. To bind the dye molecules to the silica shell, the Au@SiO_2 NPs were functionalized with (3-aminopropyl)triethoxysilane (APTES) to obtain an amine-modified nanoparticle surface (Figure 2A). A concentration equivalent to 4 APTES monolayers per NP was used in the functionalization step. The zeta potential of the silica-coated gold particles changes from negative to positive following the surface functionalization (Figure 2B).

To attach the fluorescent dye, *N*-hydroxysuccinimide (NHS)-modified dye molecules were allowed to react with the amine-capped gold particles. Both surface functionalization with APTES and the dye-coupling reaction were carried out in ethanol as the amine-capped Au@SiO_2 NPs exhibited higher colloidal stability in ethanol than in water.[26] Dye attachment yields above 80% were routinely obtained in ethanol because the hydrolysis of the reactive NHS moiety on the dye is much slower in ethanol than in water.

A change in silica shell thickness before and after the functionalization could not be detected from TEM image analysis (see Supporting Information Figure S6). Only five dyes per nanoparticle were used in the coupling reaction, and a high NP concentration between 50 and 100 nM was necessary to obtain an average degree of labeling of about 75%. Generally, the attachment was more efficient for particles with a thicker silica shell due to the higher surface area and the increased number of binding sites available per particle. To verify that the dye was indeed bound to the NP surface and not only adsorbed electrostatically or nonspecifically, carboxylic acid instead of NHS-modified dyes were used in an otherwise identical attachment procedure. Less than 5% of the dyes were found to attach to the nanoparticle surface in this control experiment. This identifies the formation of an amide bond between the dye's reactive NHS group and the surface confined amine moieties to be the major attachment mechanism.

Dye–Dye and Dye–Surface Interactions. Changing the local environment of a dye molecule, for example by binding it to a surface, or locating many dye molecules in close proximity to one another can both significantly affect the dye luminescence. Electronic charge in general[27] and amines in particular[28,29] are known to affect the fluorescence of nearby dye molecules. The confinement of several dyes to the surface of a nanoparticle leads to a significant local increase in dye concentration. This facilitates multimer formation between dyes, which can lead to significant fluorescence quenching. Therefore, APTES functionalized silica particles (50 nm diameter) were used in control experiments to determine (i) whether the binding of the dye to an amine-modified silica surface affects the fluorescence and (ii) how many dyes can be bound to one silica particle before dye–dye interactions between the adsorbed fluorophores dominate the observed fluorescence signals.

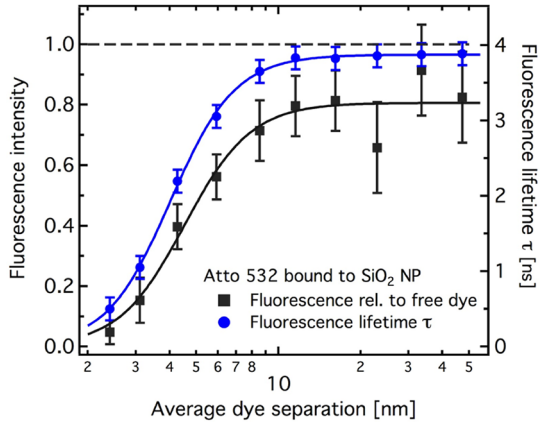

Figure 3. Steady-state fluorescence intensity (black squares) and fluorescence lifetime (blue circles) of the dye Atto 532 bound to a silica nanoparticle of 50 nm diameter as a function of the average separation between dyes on the nanoparticle surface. The shortest (2.4 nm) and largest (47 nm) average dye separations correspond to 1350 and 3.5 dyes bound to one nanoparticle on average, respectively. The highest dye concentration used in any experiment was 2.5 μM. The dashed horizontal line indicates both steady-state fluorescence intensity and fluorescence lifetime of the free dye in solution. The solid lines are a guide to the eye only.

Figure 3 shows that both the binding itself as well as the number of dyes bound to one particle affect the fluorescence and the fluorescence lifetime relative to a free dye in solution. For average dye separations above 15 nm (less than 30 dyes per particle), only the effect of the dye's surface confinement is seen resulting in a small (<5%) decrease in fluorescence lifetime and in a 20% decrease in steady-state fluorescence relative to the fluorescence of the free dye. A very pronounced decrease in both fluorescence intensity and lifetime is observed for dye separations below 10 nm (more than 75 dyes per particle). For the highest dye loading, the steady-state fluorescence decreases by more than 90% and the fluorescence lifetime is reduced to 0.5 ns compared to 4.0 ns for the free dye in solution.

A possible cause for the observed fluorescence intensity quenching and lifetime shortening is the interplay of the existence of trap states and homo-Förster resonance energy transfer (homo-FRET). At short average dye separations, trap states are created on the NP surface for example through the formation of weakly fluorescent dimers. Even at the shortest average dye separations, only a fraction of the dye molecules on the NP surface will create trap states. At these separations however, energy can be transferred efficiently between neighboring fluorophores *via* homo-FRET, for which the Förster radius of Atto 532 is $r_0 = 5.8$ nm[25] (see Supporting Information Figure S15 for a comparison between calculated FRET efficiencies and the observed quenching). Homo-FRET alone is not expected to alter the fluorescence properties of the dye molecule. Nonetheless, in combination with the existence of trap states, homo-FRET can enhance the effect of trap states and explain the significant decrease in fluorescence intensity and lifetime: At dye separations below 5.8 nm excitation energy is transferred very efficiently between dye molecules until it dissipates nonradiatively upon transfer to a trap state. However, the unambiguous identification of the cause of this pronounced decrease in fluorescence intensity and lifetime is beyond the scope of this work. The result is nonetheless very important since it clearly demonstrates the importance of a close control over the number of dyes bound to each particle. For the assumption $k_{dd} \approx 0$ to be valid, dyes must be separated by more than 15 nm on the nanoparticle surface. For the smallest particle used in this study (20 nm diameter), this means that no more than about five dyes can be bound to each NP.

Another possible de-excitation mechanism is charge transfer between dye and gold nanoparticle. However, SiO_2 is used as an insulating material in various micro- and nanoelectronic devices[30] and even ultrathin films below 5 nm thickness are known to conduct electronic charge poorly unless bias voltages, sufficient to change the atomic structure of the films, are applied.[31] We therefore assume this mechanism to be negligible.

EXPERIMENTS

One big experimental challenge for the determination of steady-state fluorescence intensities of fluorescent dyes in the presence of gold nanoparticles is that the molar extinction coefficient at the surface plasmon peak even of small Au NPs (<20 nm) is 3 orders of magnitude higher than those of the adsorbed dye molecules at their respective absorption maxima. The fact that only a maximum of five dye molecules can be bound to one particle to prevent dye–dye energy transfer means that the problem cannot be solved by using a large molar excess of dyes in the experiments. One strategy to circumvent this problem is to use dyes, which absorb at wavelengths above 620 nm where the Au NP extinction is about 1 order of magnitude weaker. However in this case, the regime where dye and Au NP extinction spectra strongly overlap and the strongest coupling is expected, cannot be investigated.

Therefore, to account for the strong effect of the Au NP extinction on excitation and emission intensities between 475 and 600 nm, the steady-state fluorescence of each sample is compared to two references (Scheme 2): "Reference 1" contains the same concentration of Au NPs and dye molecules and the only difference to the sample is that the dyes are not attached to the NP. Thereby, the high optical density of the gold nanoparticles in general and the light scattering of the Au@SiO_2 NPs with a thicker silica shell in particular are accounted for experimentally. A silica nanoparticle was used as a second reference sample

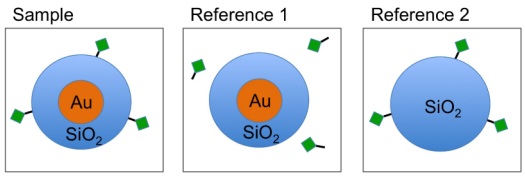

Scheme 2. Schematic representation of a typical sample and the corresponding reference samples. For each sample, a reference sample with the same concentration of dyes and Au NPs was prepared, where the dyes were not bound to the NP surface (Reference 1). Reference 2 was used to account for the effect of the dye's confinement to an amine modified silica surface.

(Reference 2) to account for fluorescence changes due to the surface confinement. The relative fluorescence intensity I_{fluo}/I_{fluo}^0 was then calculated from the "Sample" and Reference 1 integrated fluorescence intensities (I_{sample} and I_{ref1}, respectively) and normalized to the fluorescence of Reference 2 relative to the free dye in solution ($I_{ref2}/I_{free\ \ dye}$) using

$$\frac{I_{fluo}}{I_{fluo}^0} = \frac{I_{sample}/I_{ref\,1}}{I_{ref\,2}/I_{free\,dye}} \tag{4}$$

(see Supporting Information for details on the data analysis). By normalizing the Sample fluorescence signal to the fluorescence of the dye attached to a silica particle (Reference 2), the intrinsic nonradiative decay rate of the dye (k_{nr}) and the influence of surface confinement (k_s) are both accounted for. Hence, the effects of the electromagnetic coupling between the Au NP and the dye molecules are isolated and I_{fluo}/I_{fluo}^0 is expected to return to unity in the absence of this coupling. Fluorescence lifetime measurements are not affected by light absorption or scattering of the Au@SiO_2 NPs. Using Reference 1-type samples verified that this is true, and this also ensured that collisional quenching between Au@SiO_2 NPs and dyes does not affect the measured lifetimes.

Theory. To interpret our experimental results, we adopt a simple model of the gold NP−dye system: The dye is described as a Hertzian dipole,[32] which is driven both by an incident (and uniform) electric field and the field reflected by the nanoparticle. The latter is calculated using Mie theory[33] assuming the gold nanoparticle to be a sphere located in an infinite homogeneous medium of refractive index 1.36 (corresponding to the solvent ethanol used in this study). The calculation of the radiative (γ_{rad}) and total (γ_{total}) decay rates relative to the same emitter at an infinite distance ($\gamma_{rad}/\gamma^0_{total}$ and $\gamma_{total}/\gamma^0_{total}$ respectively) follows the model derived by Kim *et al.*,[34] which has recently been discussed and employed in a number of publications.[35−38] We note that this approach is an exact one within the two main approximations we have made (see Supporting Information) and we further note that the model by Gersten and Nitzan is a special case of the one presented here. Importantly, within this model the dipole emitter in free space can only decay *via* emission of radiation, implying that in the absence of a gold nanoparticle, this dipole has a quantum yield of unity (and thus exhibits a total decay rate which equals the radiative decay rate, *i.e.* $\gamma^0_{rad} = \gamma^0_{total}$). Calculated are the radiative and total decay rate relative to a molecular emitter at an infinite distance to the gold nanoparticle, $k_{rad} = \gamma_{rad}/\gamma^0_{total}$ and $k_{total} = \gamma_{total}/\gamma^0_{total}$, respectively. In both cases, normal and tangential dye orientations with respect to the nanoparticle surface ($k_{rad}^{\perp}$, $k_{total}^{\perp}$ and $k_{rad}^{\parallel}$, $k_{rad}^{\parallel}$) are evaluated separately at the experimental emission maximum of each dye (Table 1). From these, values for a statistical dye orientation are calculated according to the geometrical average $\langle X\rangle = (X^{\perp} + 2X^{\parallel})/3$[39] and are referred to as "Theory average". This geometrical averaging is reasonable here as the dye's transition dipole moment will in general neither be exactly normally nor tangentially oriented to the nanoparticle surface, but at a variable angle due to the position and the flexibility of the carbon chain linker (see Supporting Information, Figure S1).

TABLE 1. Optical Properties of the Fluorophores Used in This Study. Absorption and Emission Peak Position Were Determined in Ethanol. The Fluorescence Quantum Yield Is Provided by the Supplier for Fluorophores in Water[25]

dye	absorption peak position [nm]	emission peak position [nm]	intrinsic quantum yield [%]
Atto 488	509	527	80
Atto 532	538	556	90
Atto 565	559	581	90
Alexa 700	710	730	25

To include the effect of the Au NP's near-field on the fluorophore's excitation rate in our theoretical model, we define the electric field enhancement I_{ex}/I_{ex}^0 as

$$\frac{I_{ex}}{I_{ex}^0} = \frac{|E(d,\omega)|^2}{|E^0(\omega)|^2} \tag{5}$$

where E and E_0 are the electric field of the incident light wave in the presence and in the absence of the gold nanoparticle, respectively, at the excitation wavelength ω and distance d from the nanoparticle surface. This enhancement factor is calculated following the approach suggested by Gaponenko *et al.*[36] (see Supporting Information for details) and evaluated at the respective experimental excitation wavelength. Radial and tangential components are again calculated separately and an average value is calculated according to the geometrical average defined in the previous paragraph. To estimate the impact of the local field enhancement on our experimental results, the enhancement was calculated for three excitation wavelengths used in experiments as a function of distance from the NP surface (Figure 4). For an excitation wavelength close to the Au NP LSPR (525 nm), the average local electric field is enhanced by a factor of

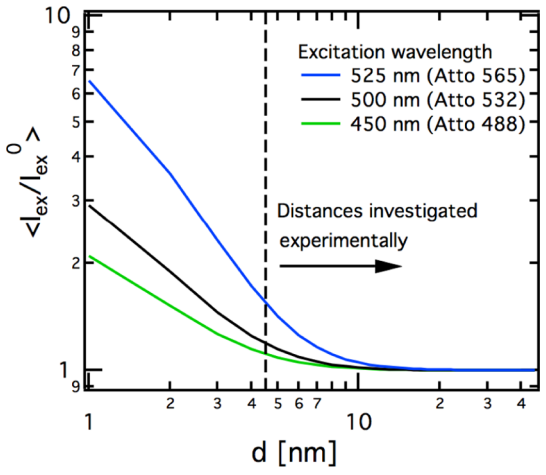

Figure 4. The average local electric field enhancement as a function of distance from the gold nanoparticle surface for three excitation wavelengths used in this study.

1.6 at the shortest dye-NP separation investigated. The enhancement decreases rapidly for larger distances d and is weaker at all distances for the other excitation wavelengths used in experiments. The average field enhancement increases rapidly for distances below 4 nm to values above 6 at a distance of 1 nm for an excitation wavelength of 525 nm. The obtained results are in good agreement with recent literature reports.[38,40]

The theoretical average relative fluorescence intensity is calculated from the quantities defined and discussed above using

$$\frac{I_{fluo}}{I_{fluo}^0} = \left\langle \frac{I_{ex}}{I_{ex}^0} \right\rangle \left\langle \frac{k_{rad}}{k_{total}} \right\rangle \quad (6)$$

which takes into account the enhanced electromagnetic near-field as well as modifications of the decay rates of the emitter due to electromagnetic coupling between molecular emitter and the gold nanoparticle. Relative fluorescence intensities for normal and tangential dye orientations are calculated according to

$$\frac{I_{fluo}^{\perp}}{I_{fluo}^{0,\perp}} = \frac{I_{ex}^{\perp}}{I_{ex}^{0,\perp}} \frac{k_{rad}^{\perp}}{k_{total}^{\perp}} \quad (7)$$

and

$$\frac{I_{fluo}^{\parallel}}{I_{fluo}^{0,\parallel}} = \frac{I_{ex}^{\parallel}}{I_{ex}^{0,\parallel}} \frac{k_{rad}^{\parallel}}{k_{total}^{\parallel}} \quad (8)$$

The impact of $\langle I_{ex}/I_{ex}^0 \rangle$ on the theoretical relative fluorescence intensities at short distances calculated from eq 6 is discussed in more detail in the Supporting Information Figure S9.

Distance Dependence. Experimental and theoretical results for the relative fluorescence intensity as a function of gold nanoparticle—dye separation d are shown in Figure 5 for the four fluorophores investigated. In all cases, the steady-state fluorescence is quenched by more than 90% at the shortest distance investigated experimentally (4.6 nm) and recovers to reference measurement values above d = 40 nm. Between these extremes the recovery of the fluorescence intensity with increasing distance is strongly wavelength dependent. The most pronounced quenching is observed for Atto 532 (Figure 5B), whose absorption peak position coincides with the Au NP LSPR. Here, I_{fluo}/I_{fluo}^0 is reduced by 95% up to a distance of 10 nm and is still significantly affected above d = 25 nm. For Alexa 700 on the other hand the fluorescence intensity recovers to 50% at d = 10 nm and is completely unaffected by the presence of the gold core for separations above 25 nm, indicating a significantly weaker electromagnetic coupling in this spectral region.

Theoretical fluorescence intensities have been calculated for a statistical orientation of the fluorophore with respect to the NP surface (Figure 5, solid lines) as well as for normally and tangentially aligned dye molecules (Figure 5, dashed lines) to illustrate the effect of the dye orientation on the predicted fluorescence intensity quenching. For Atto 532, Atto 565, and Alexa 700, the theoretical prediction for a statistical dye orientation is in excellent quantitative agreement with the observed quenching at all distances. In the case of Atto 488, the theoretical results obtained for a tangential dye orientation show the best agreement with experimental results. This suggests that the preferred orientation of Atto 488 is tangential to the NP surface, possibly due to the formation of hydrogen bonds between the primary amine side groups of Atto 488 with the primary amines of APTES on the NP surface (see Supporting Information for the chemical structures of the dye molecules). Interestingly, our model also predicts that the strongest orientation dependence of the fluorescence intensity quenching will occur for Atto 488. While the fluorescence intensity of a normally oriented emitter is quenched by about 70% at a distance of 21 nm, that of a tangentially oriented fluorophore is only quenched by about 30% at the same distance. In the case of Alexa 700 on the other hand, the predicted quenching only weakly depends on the emitter orientation at most distances.

A decrease in fluorescence intensity can be caused by a decrease in the radiative rate, an increase in the nonradiative rate or a change in both (eq 1). From changes in the fluorescence intensity alone, one cannot separate radiative and nonradiative contributions. Therefore, the relative fluorescence lifetime was determined as a function of the Au NP-dye separation d for all dye molecules as well (Figure 6A–D). τ and τ^0 refer to the fluorescence lifetime of the fluorophore bound to a Au@SiO_2 NP and a silica nanoparticle, respectively. See Supporting Information Figure S12 for raw data and analysis of the time-resolved fluorescence decay measurements. For short distances below 8 nm, the lifetime of all fluorophores decreases by 80% or more,

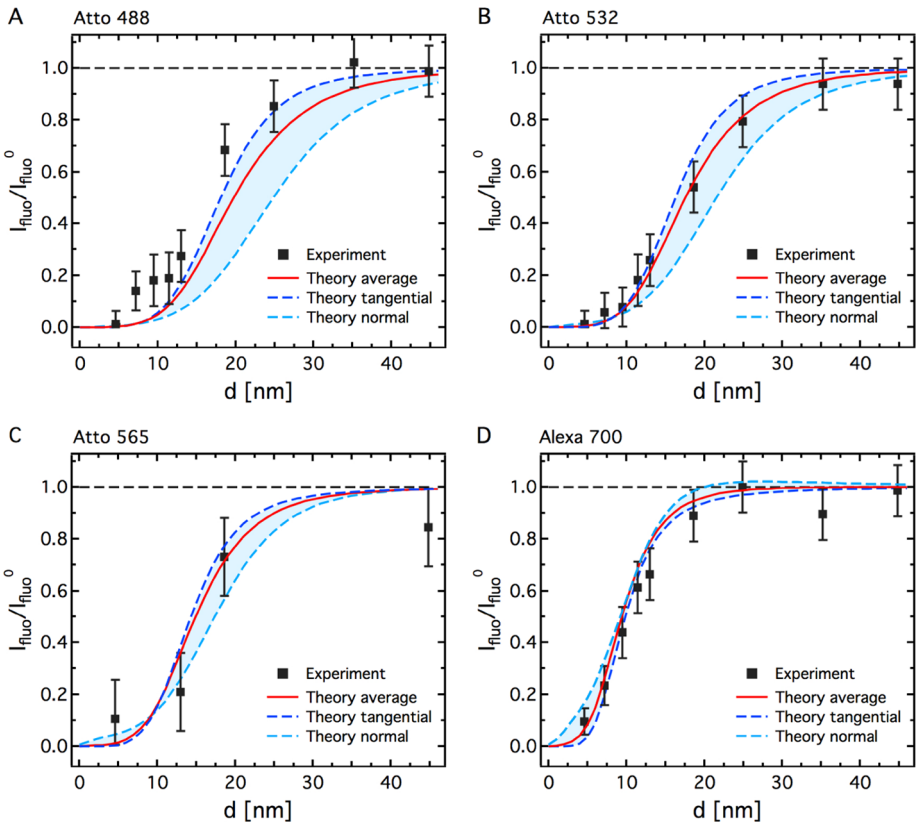

Figure 5. Experimental (black squares) and theoretical (solid and dashed lines) results for the relative fluorescence intensity as a function of the nanoparticle−dye separation *d*. The fluorophores shown are Atto 488 (A), Atto 532 (B), Atto 565 (C), Alexa 700 (D). Experimental and averaged theoretical results were obtained using eqs 4 and 6, respectively. Theoretical relative fluorescence intensities for normal and tangential dye orientations (dashed lines) were calculated using eqs 7 and 8.

and recovers to reference measurement values for separations above 40 nm. The trend in the recovery of the fluorescence lifetime with increasing distance closely resembles the one observed for the relative fluorescence intensities in Figure 5, that is, the influence of the gold nanoparticle is most pronounced for Atto 488 and Atto 532 and significantly weaker in the case of Alexa 700. Also shown in Figure 6 are the relative fluorescence lifetimes predicted by our model, which we assume to be equal to the inverse of the relative total decay rate according to

$$\frac{\tau}{\tau^0} = \frac{1}{\langle k_{total} \rangle} \qquad (9)$$

The normal and tangential components of the relative fluorescence lifetime are calculated from $1/k_{total}^{\perp}$ and $1/k_{total}^{\parallel}$, respectively. The theoretical average of τ/τ^0 is in good quantitative agreement with the experimental values obtained for Atto 532, Atto 565, and Alexa 700 with only small deviations at large distances in the case of Atto 565. The experimental fluorescence lifetimes of Atto 488 are in excellent quantitative agreement with the theoretical predictions for a tangentially oriented emitter, also pointing toward a preferred tangential orientation of Atto 488.

Our results are in agreement with recent studies on gold nanoparticle induced fluorescence quenching.[12−16] Since the coupling between Au NP and dye strongly depends on the nanoparticle size,[15,35] we can only compare our findings to literature results obtained for gold particles of comparable size. In the spectral region above 600 nm our experimental results are in good agreement with a very recent study by Tinnefeld *et al.*[13] based on single molecule experiments where only one dye molecule was used per Au NP, which excludes dye−dye interactions as a cause for the observed quenching. Feldmann *et al.* report quenching efficiencies of about 50% for another dye absorbing in the red part of the spectrum (Cy5) for NP-dye separations up to 16 nm.[15] The more pronounced quenching observed by Feldmann *et al.* compared to the results obtained by Tinnefeld *et al.* may be due to dye−dye interactions, which can be significant as we have demonstrated in this report. In the spectral region between 500 and 600 nm quenching efficiencies above 90% have been reported for NP−dye separations below 5 nm,[14] which is in agreement with our observations. The lifetime shortening reported by Sandoghdar *et al.*[12] based on single molecule experiments for Atto 532 attached to an Au NP through double-stranded DNA are also in qualitative agreement with our results. The quenching observed by Liu and Lindsay *et al.* in ensemble measurements is in qualitative agreement with our findings as well.[16]

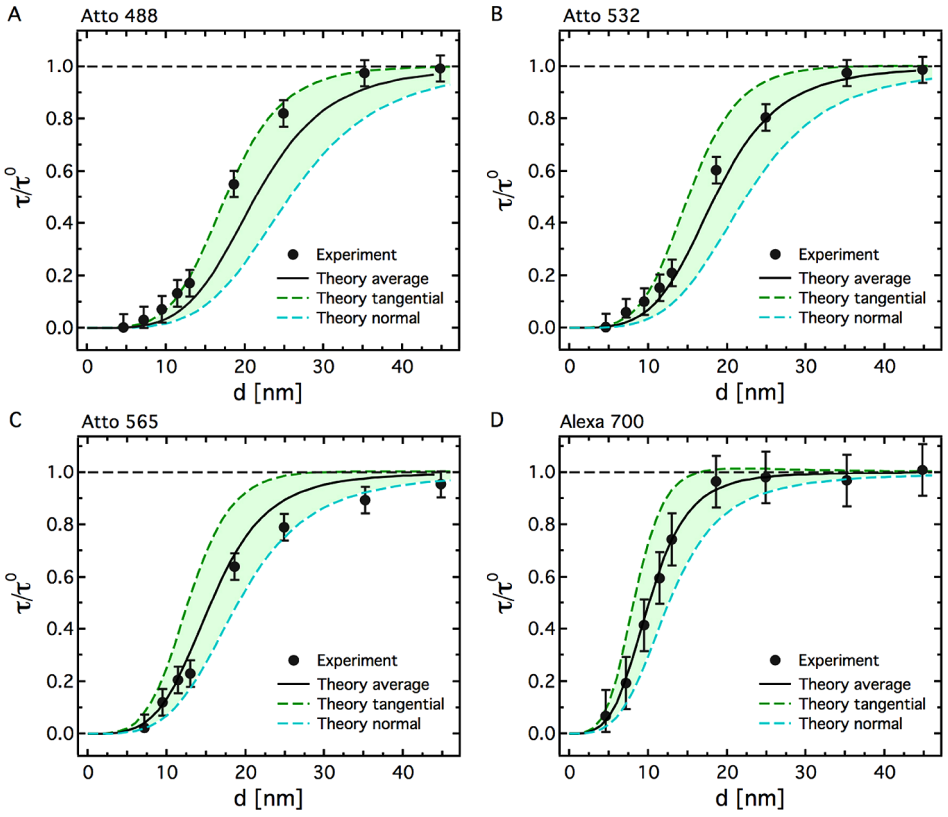

Figure 6. Relative fluorescence lifetime τ/τ^0 as a function of distance d between dye and gold nanoparticle. τ^0 is the fluorescence lifetime of the dye molecule bound to a silica NP, which is slightly shorter than the lifetime of the free dye in solution. Theory averages were calculated from eq 9 and the corresponding normal and tangential component as $1/k_{total}^{\perp}$ and $1/k_{total}^{\parallel}$. The τ^0 values for the different dyes are: (A) Atto 488: 4.1 ns, (B) Atto 532: 4.0 ns, (C) Atto 565: 4.1 ns, and (D) Alexa 700: 1.8 ns. See Supporting Information Table S9 for the fluorescence lifetimes of the free dyes in solution.

NSET theory was found to strongly underestimate the observed quenching in agreement with the findings of Tinnefeld *et al*. This is reasonable as the theory was developed for metal surfaces only and does not take into account the occurrence of nanoparticle LSPRs. Nonetheless, the general $1/d^4$ distance dependence was found to describe the experimental results obtained here well. See Supporting Information for a comparison between our results and NSET theory (Figure S11) and a $1/d^4$ distance dependence (Figure S10).

From the experiments presented here, a strict separation of an increase in the dye's "intrinsic" nonradiative decay rate (the direct conversion of an electronically excited state to phonons) from an increasing rate of energy transfer is not possible. However, considering that the dyes are attached to the same surface through the same functional groups it is reasonable to assume that the intrinsic nonradiative decay of the dye does not change as a function of the Au NP–dye distance d. It is therefore instructive to derive relative decay rates from the measured relative fluorescence intensity and fluorescence lifetime τ/τ^0 (both of which are corrected for intrinsic radiationless decay) using the calculated field enhancement factor $\langle I_{ex}/I_{ex}{}^0\rangle$. Assuming k_{nr} to be negligible and in accordance with our dipole model for the dye, we use

$$\frac{I_{fluo}}{I^0_{fluo}} = \left\langle \frac{I_{ex}}{I^0_{ex}} \right\rangle \frac{k_{rad}}{k_{rad} + k_{et}} \tag{10}$$

to compare experimental and theoretical decay rates. The experimental relative radiative rate can then be calculated from the equation:

$$k_{rad} = \frac{I_{fluo}/I^0_{fluo}}{\langle I_{ex}/I^0_{ex}\rangle(\tau/\tau^0)} \tag{11}$$

The rate of energy transfer between the Au NP and a nearby dye molecule is calculated from the difference between total and radiative contributions:

$$k_{et} = k_{total} - k_{rad} \tag{12}$$

where k_{total} is given experimentally by τ^0/τ. Using this equation the rate of energy transfer can be calculated for our model as well. In this model, the term "energy transfer" is well-defined and refers to the damping of the emitter oscillation through electromagnetic coupling to the gold nanoparticle. This coupling results in the excitation of higher-order (non-dipolar) resonant modes in the nanoparticle, which decay into phonons and eventually result in joule heating. Hence, in the model fluorescence enhancements are represented by increases in the relative radiative decay rate or the

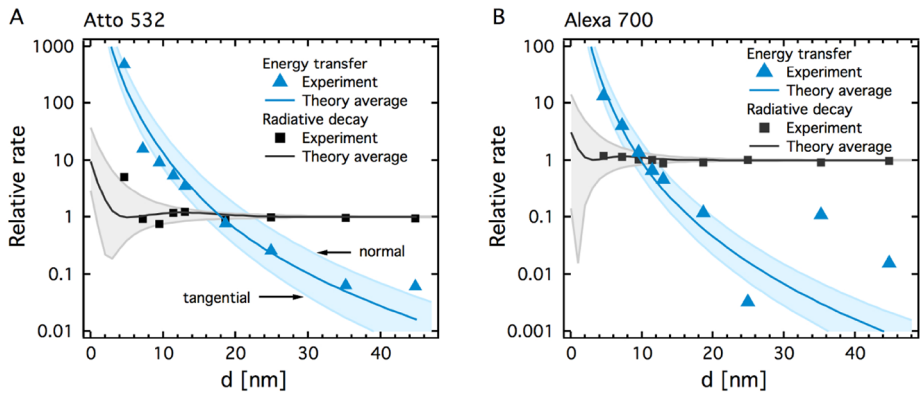

Figure 7. Relative radiative and energy transfer rates determined experimentally (symbols) and calculated (solid lines) for Atto 532 (A) and Alexa 700 (B) as a function of the distance *d* between Au NP and dye. Energy transfer from the dye emitter to the gold nanoparticle causes the pronounced increase in the rate of energy transfer with decreasing distance (see main text for Discussion). Relative experimental radiative decay and energy transfer rates were determined from eqs 11 and 12, respectively. The averaged theoretical counterparts were calculated accordingly as $\langle k_{rad}\rangle = \langle Q/Q^0\rangle\langle k_{total}\rangle$ and $\langle k_{et}\rangle = \langle k_{total}\rangle - \langle k_{rad}\rangle$. The upper and lower bounds of the theory traces represent the results for a normal and tangential dye orientation respectively in all cases.

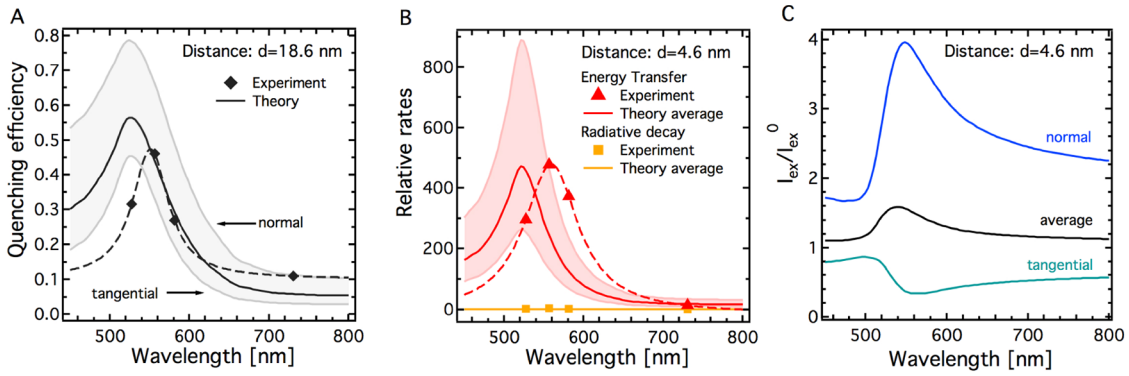

Figure 8. Wavelength dependence of the quenching efficiency (A), the relative energy transfer rate k_{et} (B), the relative radiative decay rate k_{rad} (B), and the calculated local field enhancement $\langle I_{ex}/I_{tx}^0\rangle$ (C). Theoretical results (solid lines) are shown as well as results calculated from experimental data (symbols). In panels A and B, the upper and lower bounds of the theoretical traces represent the results for a normal and tangential orientation of the fluorophore, respectively. Dashed lines are a guide to the eye only.

locally enhanced electric near-field and fluorescence quenching by the relative rate of energy transfer. A detailed description of experimental and theoretical quantities and their assumed relation is given in the Supporting Information.

Experimentally and theoretically determined relative radiative and energy transfer rates for Atto 532 and Alexa 700 are shown in Figure 7 panels A and B, respectively. Interestingly the radiative rate is largely unaffected by the presence of the gold nanoparticle for distances between 15 and 44 nm and increases by about 1 order of magnitude at shorter distances. Conversely, energy transfer starts above $d = 20$ nm and increases superexponentially with decreasing distance by a total of about 4 orders of magnitude. This highly efficient energy transfer determines the observed steady-state fluorescence quenching and the excited state lifetime shortening at smaller distances—despite an increase in the radiative decay rate. Both the comparatively weak distance dependence of the radiative rate and the drastic increase in the rate of energy transfer for decreasing Au NP−dye separations are predicted by our model and are in good agreement with experiment. Despite the apparently similar increase in the relative energy transfer rate for Atto 532 and Alexa 700 it is important to note that the scales in Figure 7A,B are offset by 1 order of magnitude. At 4.6 nm, both the theoretical and experimentally observed energy transfer rates are about 30 times more efficient in the case of Atto 532 compared to Alexa 700.

Wavelength Dependence. The spectral separation between the fluorophore emission and the Au NP absorption is the second most important parameter determining the electromagnetic coupling between fluorophore and gold nanoparticle. Therefore, the quenching efficiency, the relative energy transfer rate, the relative radiative rate, and the near-field enhancement have been calculated as a function of wavelength and are compared to experimental results in

Figure 8A–C. The quenching efficiency is here defined as $1 - I_{fluo}/I_{fluo}^{0}$ and was evaluated at a distance of d = 18.6 nm (Figure 8A). Our model predicts the strongest quenching for a fluorophore emitting exactly at the spectral position of the Au NP LSPR at 525 nm, while the strongest quenching is observed for Atto 532 in experiments. The theoretical quenching efficiency closely follows the plasmonic absorption characteristics of the Au@SiO_2 NPs (see Supporting Information Figure S13 for a graphical comparison). The wavelength dependence of k_{et}, k_{rad} and $\langle I_{ex}/I_{ex}^{0} \rangle$ is investigated at a distance of 4.6 nm and shows that energy transfer from the fluorophore to the Au NP is the dominant decay mechanism at all wavelengths, causing the pronounced quenching of the fluorescence intensity and lifetime at short dye—NP separations. Compared to the relative energy transfer rates, the experimental and theoretical values of k_{rad} remain at values between 1 and 5 over the whole spectral range investigated. Also a 1.6-fold enhanced average local electric near-field at 540 nm has no significant effect on the observed fluorescence intensity due to the highly efficient energy transfer. The strongest electromagnetic coupling is observed for a normal fluorophore orientation in our model. From the experimental results presented in this study, it cannot be excluded that the observed wavelength dependence of the fluorescence quenching is also partially caused by the differences in intrinsic quantum yield between the dyes used.

CONCLUSION

Au@SiO_2 core–shell nanoparticles were used to systematically study the electromagnetic coupling between a fluorophore and 13 nm diameter gold nanoparticles *via* steady-state and time-resolved fluorescence spectroscopy. For a spherical gold particle of a given size, this coupling is known to critically depend on two parameters: the distance between the gold nanoparticle and the dye emitter, and the wavelength of the emitter with respect to the gold nanoparticle LSPR. Both parameters were varied and investigated experimentally and theoretically, yielding three major results. (1) Our theoretical model quantitatively predicts the observed quenching of the steady-state fluorescence and shortening of the fluorescence lifetime. The quenching is caused by energy transfer from the molecular emitter to higher-order localized surface plasmon modes in the gold nanoparticle. (2) The most efficient energy transfer (and resulting quenching) occurs for an emitter wavelength, 30 nm red-shifted from the gold nanoparticle LSPR. Quenching is more than 40% less efficient for the near-infrared fluorophore with ca. 200 nm red-shifted emission at 730 nm. (3) In the absence of a metal nanoparticle, dye–dye interactions between fluorophores attached to silica nanoparticles can decrease the fluorescence of the fluorophores by more than 90%. For the fluorophore Atto 532, these interactions start to significantly reduce the observed fluorescence intensities and lifetimes for average dye separations below 10 nm.

METHODS

Au@SiO_2 Nanoparticles and Fluorescent Dyes. Au nanoparticles were synthesized using the Turkevich method. Silica shells were grown following the procedure reported by Liz-Marzan *et al.*[41] For typical TEM images for all silica shell thicknesses see Supporting Information Figure S4. Atto and Alexa dye molecules were purchased from Atto-Tec, Germany and Invitrogen, USA, respectively, and used as received. See Supporting Information for details on NP functionalization and dye attachment.

Nanoparticle-Dye Coupling Reaction. Dye stock solutions (0.2–1 mM) were prepared and stored under nitrogen atmosphere in dimethyl sulfoxide (Sigma-Aldrich, USA) to prevent the hydrolysis of the dyes' reactive NHS group. Aliquots thereof were prepared and diluted in an ethanoic solution of Tween20 (0.05 wt %, Sigma-Aldrich, USA) to the desired concentration before each dye attachment step, which was carried out under ambient conditions. Au@SiO_2 NP solutions were concentrated (50–150 nM nanoparticle concentration) to create favorable conditions for the NHS–NH_2 coupling reaction. In a typical dye coupling reaction, the dye solution (10 μL) was added to the NP solution (30 μL) under sonication to ensure a fast concentration equilibration. The mixture was allowed to react for 3 h and then diluted 40 times in ethanol (0.05 wt % Tween20). See Supporting Information for details on the preparation of samples and their references for the different measurements.

Zeta-Potential Measurements. A Zeta Sizer nano ZS (Malvern Instruments Ltd., UK) was used to determine zeta potentials of functionalized and unfunctionalized nanoparticles in ethanol.

Optical Spectroscopy. Absorption and steady-state fluorescence spectra were obtained using a Lambda-950 UV–vis absorption spectrometer (Perkin-Elmer, USA) and a Fluoromax 4 fluorometer (Horiba, Japan), respectively. Fluorescence decay histograms were recorded *via* time correlated single photon counting (TCSPC). A picosecond pulsed supercontinuum fiber laser (Fianium, SC 400-4-pp) was used as a exciation source. The excitation wavelength was selected by using appropriate bandpass filters (Chroma, USA). Emission from the sample was collected at a 90° angle with respect to the excitation beam, passed through a monochromator (Digikröm DK480, Spectral Products, USA) and focused onto a fast response avalanche photodiode detector (ID-100, IDQuantique, Switzerland). Photon emission times were recorded by a photon counting module (PicoHarp 300, Picoquant, Germany). The time-resolved traces were analyzed by a nonlinear least-squares iterative deconvolution based on the Levenberg–Marquardt algorithm. For raw data, experimental and data-analysis details see Supporting Information.

Conflict of Interest: The authors declare no competing financial interest.

Supporting Information Available: Chemical structures of the fluorescent dyes; absorption and emission spectra of all fluoropores; TEM images of all Au@SiO_2 NPs; silica shell thicknesses with standard deviations; extinction spectra of all Au@SiO_2 NPs in solution; influence of APTES functionalization on silica shell thickness; influence of Tween20 on Au@SiO_2 NP zeta potential. Experimental and analysis details: sample preparation, steady-state and fluorescence decay measurements; nomenclature and definitions used in our theoretical model; equations and parameters used for the numerical evaluation of the model; influence of near-field on calculated relative fluorescence intensities; power law fits to the distance dependent fluoresence

intensity quenching; NSET calculations and comparison to measured values; fluorescence decay raw data. This material is available free of charge *via* the Internet at http://pubs.acs.org.

Acknowledgment. The authors would like to acknowledge the ARC for providing equipment (LE0883019) and fellowship (DP110105312) support. This work was further supported by the Australian Solar Institute, the Victorian State Government (DBI-VSA and DPI-ETIS) and Monash University as well as the Commonwealth Scientific and Industrial Research Organization through an OCE Science Leader position. This work was performed in part at the Melbourne Centre for Nanofabrication, an initiative partly funded by the Commonwealth of Australia and the Victorian Government. D.G. would like to acknowledge the ARC for support through DP110101767. The authors thank A. Funston for valuable discussions and B. Greystone for assistance with the time correlated single photon counting measurements. The authors acknowledge use of facilities and the assistance of E. Lavoie and L. Bourgeois within the Monash Centre for Electron Microscopy.

REFERENCES AND NOTES

1. Pelton, M.; Aizpurua, J.; Bryant, G. Metal-Nanoparticle Plasmonics. *Laser & Photonics Rev.* **2008**, *2*, 136–159.
2. Kelly, K. L.; Coronado, E.; Zhao, L. L.; Schatz, G. C. The Optical Properties of Metal Nanoparticles: The Influence of Size, Shape, and Dielectric Environment. *J. Phys. Chem. B* **2003**, *107*, 668–677.
3. Maier, S. A.; Kik, P. G.; Atwater, H. A.; Meltzer, S.; Harel, E.; Koel, B. E.; Requicha, A. A. G. Local Detection of Electromagnetic Energy Transport Below the Diffraction Limit in Metal Nanoparticle Plasmon Waveguides. *Nat. Mater.* **2003**, *2*, 229–232.
4. Atwater, H. A.; Polman, A. Plasmonics for Improved Photovoltaic Devices. *Nat. Mater.* **2010**, *9*, 205–213.
5. Liu, Z.; Hou, W.; Pavaskar, P.; Aykol, M.; Cronin, S. B. Plasmon Resonant Enhancement of Photocatalytic Water Splitting Under Visible Illumination. *Nano Lett.* **2011**, 1111–1116.
6. Lakowicz, J. R. Plasmonics in Biology and Plasmon-Controlled Fluorescence. *Plasmonics* **2006**, *1*, 5–33.
7. Kamat, P. V. Meeting the Clean Energy Demand: Nanostructure Architectures for Solar Energy Conversion. *J. Phys. Chem. C* **2007**, *111*, 2834–2860.
8. Lakowicz, J. R.; Fu, Y. Modification of Single Molecule Fluorescence Near Metallic Nanostructures. *Laser Photonics Rev.* **2009**, *3*, 221–232.
9. Anger, P.; Bharadwaj, P.; Novotny, L. Enhancement and Quenching of Single-Molecule Fluorescence. *Phys. Rev. Lett.* **2006**, *96*, 113002.
10. Bharadwaj, P.; Novotny, L. Spectral Dependence of Single Molecule Fluorescence Enhancement. *Opt. Express* **2007**, *15*, 14266–14274.
11. Kühn, S.; Håkanson, U.; Rogobete, L.; Sandoghdar, V. Enhancement of Single-Molecule Fluorescence Using a Gold Nanoparticle as an Optical Nanoantenna. *Phys. Rev. Lett.* **2006**, *97*, 017402.
12. Seelig, J.; Leslie, K.; Renn, A.; Kühn, S.; Jacobsen, V.; van de Corput, M.; Wyman, C.; Sandoghdar, V. Nanoparticle-Induced Fluorescence Lifetime Modification as Nanoscopic Ruler: Demonstration at the Single Molecule Level. *Nano Lett.* **2007**, *7*, 685–689.
13. Acuna, G. P.; Bucher, M.; Stein, I. H.; Steinhauer, C.; Kuzyk, A.; Holzmeister, P.; Schreiber, R.; Moroz, A.; Stefani, F. D.; Liedl, T.; *et al.* Distance Dependence of Single-Fluorophore Quenching by Gold Nanoparticles Studied on DNA Origami. *ACS Nano* **2012**, *6*, 3189–3195.
14. Dulkeith, E.; Morteani, A.; Niedereichholz, T.; Klar, T.; Feldmann, J.; Levi, S.; van Veggel, F. C.; Reinhoudt, D.; Möller, M.; Gittins, D. Fluorescence Quenching of Dye Molecules Near Gold Nanoparticles: Radiative and Nonradiative Effects. *Phys. Rev. Lett.* **2002**, *89*, 203002.
15. Dulkeith, E.; Ringler, M.; Klar, T. A.; Feldmann, J.; Muñoz Javier, A.; Parak, W. J. Gold Nanoparticles Quench Fluorescence by Phase Induced Radiative Rate Suppression. *Nano Lett.* **2005**, *5*, 585–589.
16. Chhabra, R.; Sharma, J.; Wang, H.; Zou, S.; Lin, S.; Yan, H.; Lindsay, S.; Liu, Y. Distance-Dependent Interactions between Gold Nanoparticles and Fluorescent Molecules with DNA as Tunable Spacers. *Nanotechnology* **2009**, *20*, 485201.
17. Schneider, G.; Decher, G.; Nerambourg, N.; Praho, R.; Werts, M. H. V.; Blanchard-Desce, M. Distance-Dependent Fluorescence Quenching on Gold Nanoparticles Ensheathed with Layer-by-layer Assembled Polyelectrolytes. *Nano Lett.* **2006**, *6*, 530–536.
18. Chowdhury, S.; Wu, Z.; Jaquins-Gerstl, A.; Liu, S.; Dembska, A.; Armitage, B. A.; Jin, R.; Peteanu, L. A. Wavelength Dependence of the Fluorescence Quenching Efficiency of Nearby Dyes by Gold Nanoclusters and Nanoparticles: The Roles of Spectral Overlap and Particle Size. *J. Phys. Chem. C* **2011**, *115*, 20105–20112.
19. Jennings, T. L.; Singh, M. P.; Strouse, G. F. Fluorescent Lifetime Quenching Near $d = 1.5$ nm Gold Nanoparticles: Probing NSET Validity. *J. Am. Chem. Soc.* **2006**, *128*, 5462–5467.
20. Tovmachenko, O. G.; Graf, C.; van den Heuvel, D. J.; van Blaaderen, A.; Gerritsen, H. C. Fluorescence Enhancement by Metal-Core/Silica-Shell Nanoparticles. *Adv. Mater.* **2006**, *18*, 91–95.
21. De Luca, A.; Grzelczak, M. P.; Pastoriza-Santos, I.; Liz-Marzan, La Deda, M.; Striccoli, M.; Strangi, G. Dispersed and Encapsulated Gain Medium in Plasmonic Nanoparticles: A Multipronged Approach to Mitigate Optical Losses. *ACS Nano* **2011**, 5823–5829.
22. Genereux, J. C.; Barton, J. K. Mechanisms for DNA Charge Transport. *Chem. Rev.* **2010**, *110*, 1642–1662.
23. Gersten, J.; Nitzan, A. Spectroscopic Properties of Molecules Interacting with Small Dielectric Particles. *J. Chem. Phys.* **1981**, *75*, 1139–1152.
24. Yun, C. S.; Javier, A.; Jennings, T.; Fisher, M.; Hira, S.; Peterson, S.; Hopkins, B.; Reich, N. O.; Strouse, G. F. Nanometal Surface Energy Transfer in Optical Rulers, Breaking the FRET Barrier. *J. Am. Chem. Soc.* **2005**, *127*, 3115–3119.
25. Atto-Tec GmbH, Siegen, Germany. Information available online at: www.atto-tec.com.
26. Graf, C.; Gao, Q.; Schütz, I.; Noufele, C. N.; Ruan, W.; Posselt, U.; Korotianskiy, E.; Nordmeyer, D.; Rancan, F.; Hadam, S.; *et al.* Surface Functionalization of Silica Nanoparticles Supports Colloidal Stability in Physiological Media and Facilitates Internalization in Cells. *Langmuir* **2012**, *28*, 7598–7613.
27. Lakowicz, J. R. *Principles of Fluorescence Spectroscopy*; Lakowicz, J. R., Ed.; Springer: New York, 2006.
28. Goodpaster, J. V; Mcguffin, V. L. Selective Fluorescence Quenching of Polycylclic Aromatic Hydrocarbons by Aliphatic Amines. *Anal. Chem.* **2000**, *72*, 1072–1077.
29. Nad, S.; Pal, H. Electron Transfer from Aromatic Amines to Excited Coumarin Dyes: Fluorescence Quenching and Picosecond Transient Absorption Studies. *J. Phys. Chem. A* **2000**, *104*, 673–680.
30. Ko, H.; Takei, K.; Kapadia, R.; Chuang, S.; Fang, H.; Leu, P. W.; Ganapathi, K.; Plis, E.; Kim, H. S.; Chen, S.-Y.; *et al.* Ultrathin Compound Semiconductor on Insulator Layers for High-performance Nanoscale Transistors. *Nature* **2010**, *468*, 286–289.
31. Houssa, M.; Nigam, T.; Mertens, P. W.; Heyns, M. M. Model for the Current–Voltage Characteristics of Ultrathin Gate Oxides after Soft Breakdown. *J. Appl. Phys.* **1998**, *84*, 4351–4355.
32. Chance, R. R.; Prock, A.; Silbey, R. Molecular Fluorescence and Energy Transfer Near Interfaces. *Adv. Chem. Phys.* **1978**, *37*, 1–65.
33. Bohren, C. F.; Huffman, D. R. *Absorption and Scattering of Light by Small Particles*; Bohren, C. F.; Huffman, D. R., Eds.; Wiley-VCH: Weilheim, Germany, 1998.
34. Kim, Y. S.; Leung, P. T.; George, T. F. Classical Decay Rates for Molecules in the Presence of a Spherical Surface: A Complete Treatment. *Surf. Sci.* **1988**, *195*, 1–14.

35. Mertens, H.; Koenderink, A.; Polman, A. Plasmon-Enhanced Luminescence Near Noble-Metal Nanospheres: Comparison of Exact Theory and an Improved Gersten and Nitzan Model. *Phys. Rev. B* **2007**, *76*, 115123.
36. Guzatov, D. V.; Vaschenko, S. V.; Stankevich, V. V.; Lunevich, A. Y.; Glukhov, Y. F.; Gaponenko, S. V. Plasmonic Enhancement of Molecular Fluorescence Near Silver Nanoparticles: Theory, Modeling, and Experiment. *J. Phys. Chem. C* **2012**, *116*, 10723–10733.
37. Zhu, J.; Li, J.-J.; Zhao, J.-W. Distance-Dependent Fluorescence Quenching Efficiency of Gold Nanodisk: Effect of Aspect Ratio-Dependent Plasmonic Absorption. *Plasmonics* **2011**, *7*, 201–207.
38. Colas des Francs, G.; Bouhelier, A.; Finot, E.; Weeber, J. C.; Dereux, A.; Girard, C.; Dujardin, E. Fluorescence Relaxation in the Near-Field of a Mesoscopic Metallic Particle: Distance Dependence and Role of Plasmon Modes. *Opt. Express* **2008**, *16*, 17654–17666.
39. Moroz, A. A Recursive Transfer-Matrix Solution for a Dipole Radiating Inside and Outside a Stratified Sphere. *Ann. Phys* **2005**, *315*, 352–418.
40. Kang, K. A.; Wang, J.; Jasinski, J. B.; Achilefu, S. Fluorescence Manipulation by Gold Nanoparticles: From Complete Quenching to Extensive Enhancement. *J. Nanobiotechnol.* **2011**, *9*, 16.
41. Liz-Marzán, L. M.; Giersig, M.; Mulvaney, P. Synthesis of Nanosized Gold−Silica Core−Shell Particles. *Langmuir* **1996**, *12*, 4329–4335.